

Research article

Numerical study of supersonic ejector with high primary flow temperature

Mohammad Reza Hashemi ¹, Behrooz Shahriari ^{2*}, Parviz Hashemi ², Mansour Asghari ²

¹PhD student, Mechanical Engineering, University of Birjand, Birjand, Iran.

²Faculty of Mechanics, Malek Ashtar University of Technology, Isfahan, Iran.

*Shahriari@mut-es.ac.ir

(Manuscript Received --- 10 Dec. 2024; Revised --- 12 Mar. 2025; Accepted --- 05 Apr. 2025)

Abstract

In this research, the performance of the supersonic ejector has been investigated numerically. Primary fluid conditions included a temperature of 520 and a pressure of 2.3 bar. The secondary fluid entered the ejector due to the very high momentum of the primary fluid and the pressure reduction caused by it. To reduce the outlet temperature of the ejector, the secondary fluid was considered with the temperature and pressure of the free atmosphere, which is equal to 288 and 1.01325, respectively. The validation results of the numerical solution revealed the use of the K- ϵ RNG turbulence model provides a satisfactory agreement between the numerical and experimental data. After passing through the oblique and expansion waves, the flow at the rear of the primary nozzle enters the mixing chamber and a strong normal shock wave is formed at the end of this area. This has led to an increase in the temperature of the ejector outlet. Also, the critical pressure value for the ejector is 0.105 MPa because increasing the outlet pressure to more than that value has caused a sharp decrease in the entrainment ratio.

Keywords: Ejector, Numerical solution, Oblique shock, Primary nozzle, Entrainment ratio.

1- Introduction

The ejector is a device that moves the secondary fluid using the momentum of the primary fluid. Ejector efficiency is lower than other fluid transfer devices. However, the advantages of the ejector are the simple structure without moving parts, low cost, and transfer of dense fluid without electrical energy. Contrary to its simple structure, the flow processes inside the ejector are complex and not fully comprehended. The lack of complete understanding of the flow processes and the dependence of the ejector performance on the geometrical changes

and operating conditions have made the design of the ejectors difficult [1]. Ejector refrigeration systems are a suitable alternative to conventional compressor refrigeration systems to reduce energy consumption [2]. In addition to cooling, ejectors are used in refrigeration systems [3], heat pumps [4], thermodynamic cycles [5], and pressure boosters in natural gas industries [6], as well as in air turbine engines [7] and rocket nozzles [8]. Theoretical studies have been carried out to examine the performance of the ejector in different operating conditions. Based on the

theory of one-dimensional fluid dynamics, the velocities of the primary and secondary flows are assumed to be uniform in their direction of movement [9]. The effect of some geometrical parameters, for example, the diameter of the primary nozzle and the mixing chamber can be checked through these models [10] [11]. Nevertheless, it should be noted that these types of theories do not have the necessary ability to determine the position of the primary nozzle outlet, the length of the mixing chamber, and the divergence angle of the diffuser part. These problems occurred due to the limitations of one-dimensional assumptions. In this case, the determining effects of the geometrical parameters on the performance of the ejector are carried out with experimental [12] [13] and numerical studies [14] [15] to acquire the optimal geometry. The first notable use of the ejector dates back to the 1800s to create vacuum pressure in the vacuum brake cylinders of trains. Then in 1902, Parsons used an ejector to create a vacuum in the steam turbine condensers. He announced the ejector as his vacuum-increasing mechanism [1]. In 1910, Maurice LeBlanc used the ejector for the first time in the ejector refrigeration cycle with water vapor as the working fluid. In the 1930s, the ejector refrigeration system gained significant attention in the air conditioning of large buildings and ships. In the second half of the last century and most cases, the ejector refrigeration system was replaced by the compressor compression refrigeration system. As a result, the research related to the ejector refrigeration system has almost stopped and focused on the vapor compression refrigeration system. In recent years, due to environmental concerns, ejector refrigeration systems have been re-considered and a lot of research has been

investigating these designs. Nowadays, in the aerospace industry, the use of an ejector is a novel idea. Ejectors with secondary fluid suction from the surrounding environment, in addition to better engine cooling, also increase thrust [16]. Therefore, major research has been done on increasing the performance of aircraft engines equipped with ejectors. Ma et al. [17] investigated the position of the ejector in a refrigeration cycle. According to operation conditions, the fluid output from the boiler determines the characteristics of the flow entering the ejector. After passing through the ejector, the flow enters the condenser section. They revealed that changes in primary flow temperature (boiler outlet flow) and secondary flow temperature can have significant effects on ejector performance. Also, the primary flow rate has increased with the increase in boiler temperature. Ruangtrakoon et al. [18] conducted an experimental study to investigate the characteristics of the inlet flows. The system design was tested at different temperatures, and the effect of flow variables was evaluated on the performance parameters of the system. The primary flow temperature was selected between 110 and 150 degrees Celsius and the effect of this temperature on the primary flow rate was studied. They concluded that for all primary nozzle shapes, increasing primary flow temperature leads to increased flow rate. Among the other things investigated in their research was the analysis of the effects of temperature change on the entrainment ratio (the ratio of the secondary flow rate to the primary flow rate) of the ejector. They demonstrated that increasing the primary flow temperature has decreased the suction ratio and increased the critical back pressure. Sun [19] investigated the operational characteristics

of the refrigeration ejector system. The operating conditions for the boiler temperature were between 95 to 135 °C and the evaporator between 5 to 15 °C. Investigations indicated that increasing the boiler temperature increases the suction ratio in the first step. However, after a certain value, higher boiler temperature has reduced the performance of the ejector. Also, higher temperatures led to enhancement of the evaporator efficiency. Finally, it can be concluded that the temperature of the evaporator has a great effect on the suction ratio and the efficiency of the ejector. Ma et al. [17], Chen et al. [16], and Zhou et al. [20] investigated the effect of secondary flow temperature changes on the ejector entrainment ratio. They illustrated that higher secondary temperature leads to an increase in the ejector critical pressure. Yen et al. [21] showed that for a constant outlet area, the ejector performance coefficient increases as the outlet temperature decreases and then reaches a constant value. Chen et al [22] by examining the one-dimensional model of the ejector concluded that the suction coefficient of the ejector increases with the reduction of the output pressure.

According to the review of the aforementioned studies, it was observed that most of the work performed on the ejector was related to the ventilation system. Since the ejector can enter the secondary fluid into the mixing chamber employing the high momentum of the primary fluid, this feature can be used for cooling purposes. In this article, the researchers introduced the ejector for cooling the rear of the aircraft engine. The secondary fluid is entered from the free atmosphere (with low temperature) into the mixing chamber and can reduce the primary fluid temperature. The ejector has been

investigated by presenting Mach, pressure, and temperature contours and graphs.

2- Numerical solution

2-1 Governing equations

Continuity, Navir-stokes, and energy equations are the general equations governing fluid flow that deal with heat transfer. These equations are presented in different forms by applying different properties of the fluid and flow such as compressibility, Newtonian, and non-Newtonian fluid. To use the equations governing the studied flow, it is first necessary to check the different properties of the flow field. The appropriate form of these equations for the studied field is presented by undertaking this. In this study, high-temperature air is studied, which is not considered due to its low-density gravity. The governing equations in the cylindrical device are presented according to the axially symmetric geometry of the ejector [23]. The cylindrical continuity equation is shown in equation (1) :

$$\frac{\partial \rho}{\partial t} + \frac{1}{r} \frac{\partial}{\partial r} (\rho r u_r) + \frac{\partial}{\partial z} (\rho u_z) = 0 \quad (1)$$

Momentum and energy equations are also shown below:

$$\rho \left(\frac{\partial u_r}{\partial t} + u_r \frac{\partial u_r}{\partial r} - \frac{u_\theta^2}{r} + u_z \frac{\partial u_r}{\partial z} \right) = -\frac{\partial p}{\partial r} + \rho g_r + \mu \left(\frac{\partial}{\partial r} \left(\frac{1}{r} \frac{\partial r u_r}{\partial r} \right) + \frac{\partial^2 u_r}{\partial z^2} \right) \quad (2)$$

$$\rho \left(\frac{\partial u_\theta}{\partial t} + u_r \frac{\partial u_\theta}{\partial r} - \frac{u_r u_\theta}{r} + u_z \frac{\partial u_\theta}{\partial z} \right) = \rho g_\theta + \mu \left(\frac{\partial}{\partial r} \left(\frac{1}{r} \frac{\partial (r u_\theta)}{\partial r} \right) + \frac{\partial^2 u_\theta}{\partial z^2} \right) \quad (3)$$

$$\rho \left(\frac{\partial u_z}{\partial t} + u_r \frac{\partial u_z}{\partial r} + u_z \frac{\partial u_z}{\partial z} \right) = -\frac{\partial p}{\partial z} + \rho g_z + \mu \left(\frac{1}{r} \frac{\partial u}{\partial r} \left(r \frac{\partial u_z}{\partial r} \right) + \frac{\partial^2 u_z}{\partial z^2} \right) \quad (4)$$

In the above equations, r , θ , and z are the coordinate directions, and the components u , μ , ρ and g are speed, dynamic viscosity, density, gravity, and turbulence kinetic energy, respectively.

2-2 k- ϵ turbulent model

k- ϵ can be considered the most famous and widely used turbulence model in solving a wide range of fluid problems, which includes several subgroups. In this model, there are two transfer equations to calculate turbulence viscosity stresses, which include turbulence kinetic energy (k) and dissipating rate (ϵ), which is shown in equations (5) and (6) [24]:

$$\frac{\partial}{\partial x_j} (\rho U_i k - \Gamma_k \frac{\partial k}{\partial x_j}) = \mu_t \left(\frac{\partial U_i}{\partial x_j} + \frac{\partial U_j}{\partial x_i} \right) \frac{\partial U_i}{\partial x_j} - \rho \epsilon \quad (5)$$

$$\frac{\partial}{\partial x_j} (\rho U_i \epsilon - \Gamma_\epsilon \frac{\partial \epsilon}{\partial x_j}) = \rho \epsilon C_1 S - \rho C_2 \frac{\epsilon^2}{k + \sqrt{\nu \epsilon}} \quad (6)$$

The parameters in this model are calibrated and established on basic experimental data such as pipe flow, flat plate, etc. [25] [26]. k- ϵ includes submodels for problems related to compressibility, buoyancy, combustion, etc.

2-3 Grid independence and numerical validation

Due to the presence of two input fluids and one output, the boundary conditions of pressure inlet and pressure outlet have been applied to input fluids (primary and

secondary fluid) and output, respectively. In all validation phases, the primary flow pressure is 1 MPa, and the secondary flow pressure is 0.5 MPa. The pressure outlet (Pd) also changes between 0.8 and 0.4 MPa. Due to the nature of the problem, the assumption of symmetry for the ejector axis has been considered and half of the model has been simulated and solved. The walls of the ejector are also selected adiabatic walls. Table 1 depicts the conditions of the numerical solution setup to perform the validation.

Table 1: Numerical solution setup to perform validation

Type of solver	pressure-based
Time	steady
Turbulent model	k- ϵ RNG
Fluid	ideal gas
Method	couple
Spatial discretization	second-order

To validate, the numerical solution has been compared with the experimental work of Chong et al. [27]. According to Fig. 1, an acceptable agreement between the present research and the experimental work is observed, for outlet pressures lower than the critical pressure. For pressures higher than the critical value, the agreement of the data was more undersized, but for the last two pressures, the data agreed reasonably with each other.

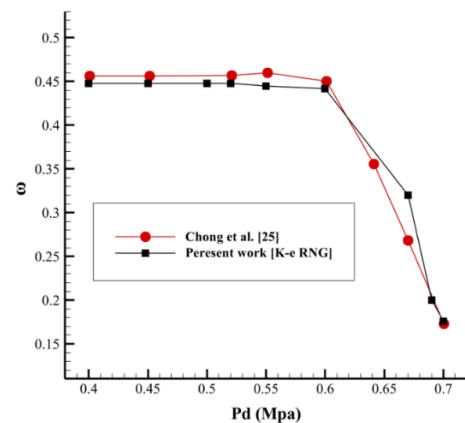


Fig. 1 Turbulent model validation

The governing equations are solved within the grids inside the ejector. As the number of these cells increases, the accuracy of the solution and the calculation time also increase. On the other hand, reducing the number of grids also reduces the calculation time and particularly the accuracy of the solution. In performing numerical solutions, declining the computational grids from a certain value onwards has not had a remarkable influence on the results. For this purpose, one should find the appropriate number of grids, which, besides preserving the accuracy of the results, minimizes the solution time. Fig. 2 demonstrates the independence of grids carried out in the present research. According to this figure, it can be seen that the number of grids increased after 60 thousand, and no specific differences appeared in the result (entrainment ratio). Also, while performing the numerical study, it was observed that this number of grids exhibited a proper convergence process and satisfied the quality requirements of meshes. Therefore, in the continuation of the research process, this number of grids has been used (Fig. 3).

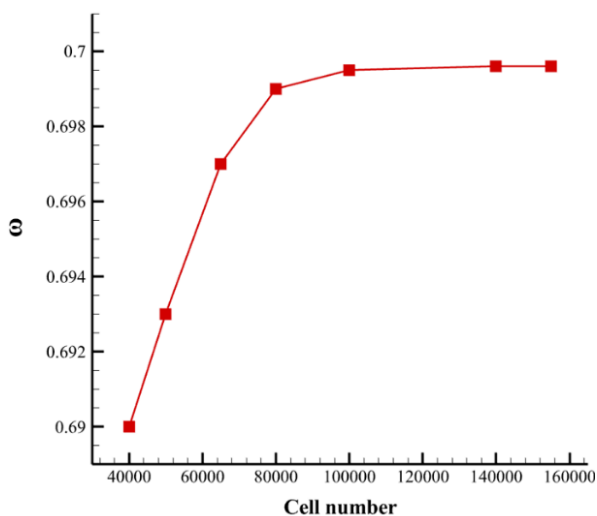


Fig. 2 The grid independence performed in the study

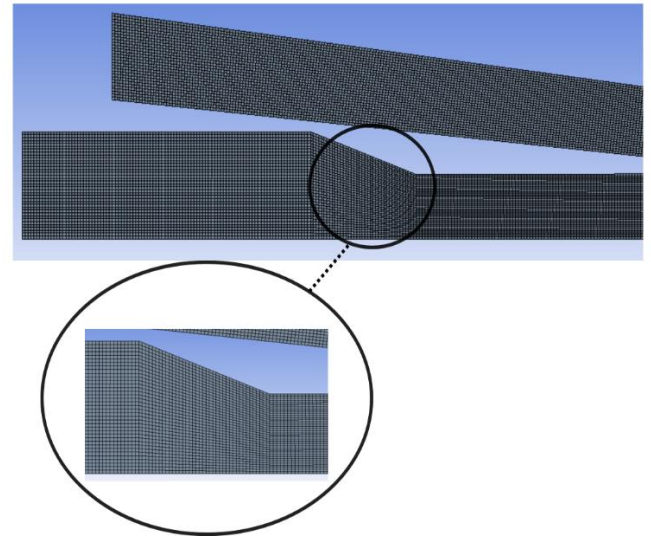


Fig. 3 Grids applied inside the ejector

3- Results and discussion

The results of the numerical solution of the ejector model are reported in this section, which is under the boundary conditions of Table 2. These results contain graphs and contours of temperature, velocity, and pressure.

Table 2: Boundary conditions used in this research

Primary flow temperature	520 K
Secondary flow temperature	288 K
Back-flow temperature	288 K
Primary flow pressure	2.3 bar
Secondary flow pressure	1.01325 bar
Back-flow pressure	1.01325 bar

Fig. 4 shows the static pressure changes along the ejector. As can be seen, there was a severe pressure drop for the ejector, which occurred at $X=0.045$ m with a value of $P_s \approx 83000$ Pa. After the first severe pressure drop, from $X=0.076$ m to $X=137$ m, there was a series of continuous pressure changes, which is a sign of subsequent oblique waves. Finally, the highest pressure drop is observed at $X=167$ m, which is due to the extreme normal shock at the end of the mixing chamber.

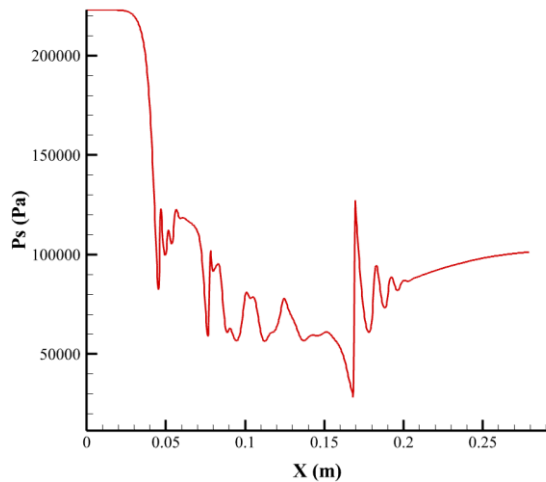


Fig. 4 Static pressure distribution along the ejector

The changes in the ejector Mach number are shown in Fig. 5. The process of changing the Mach number is such that at $X=0.042$ m the flow reached supersonic and thus, a very small reduction was observed in the Mach number. Then up to $X=0.167$ m by passing through several shock waves, it has reached the highest Mach number in this place ($M=2.02$). Thus, a sharp drop in Mach number occurred to $M=0.5$ at $X=0.169$ m. This sharp decrease in Mach number from supersonic to subsonic can be related to normal shock waves.

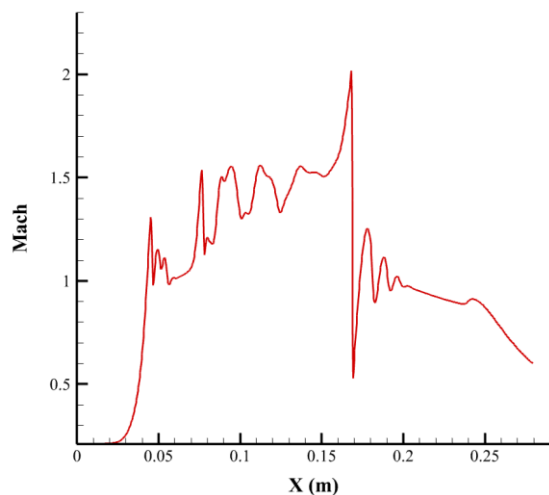


Fig. 5 Mach distribution along the ejector

According to Fig. 6, the flow entered the primary nozzle with a subsonic speed and reached speeds higher than the speed of

sound upon reaching the throat. At the outlet of the primary nozzle, an increase in the flow Mach number is observed due to the formation of the expansion shock. This process of raising the Mach number and creating oblique and expansion shocks existed until the latest portion of the mixing chamber, which can be seen in Fig. 7. Then, at the entrance of the diffuser, a high-intensity normal shock occurred inside the ejector, after which the free stream velocity reached the subsonic. The core of the jet flow for this model is smaller from the initial nozzle outlet to the end of the mixing chamber. This is due to the suction of the secondary fluid and the interaction of this flow with the core of the main jet. In fact, the high energy and momentum of the core of the main jet gradually decrease with the suction of the secondary fluid.

Fig. 8 shows the temperature contour. According to it, continuous temperature changes have occurred in the primary nozzle of the ejector, and these temperature fluctuations are due to the shock waves created in this area. This temperature reduction process continued until the end of the mixing chamber and formed a normal shock in the ejector (Fig. 9). After that, there was a sharp temperature rise. Also, the entering of the secondary flow into the mixing chamber led to a decrease in the wall temperature until the last portion of the mixing chamber. It is seen that the suction of the secondary flow in the mixing chamber causes the main jet core to become smaller in the center of the ejector. The increment temperature after the normal shock has increased the exit temperature from the center of the ejector.

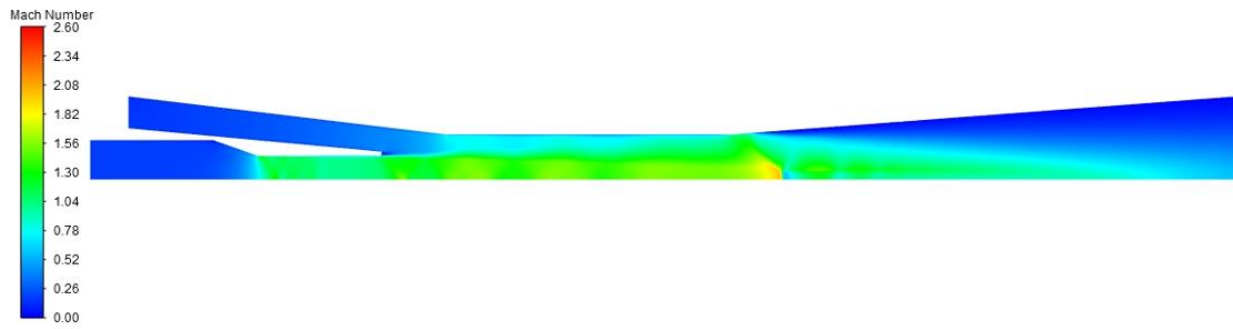


Fig. 6 Ejector Mach number contour

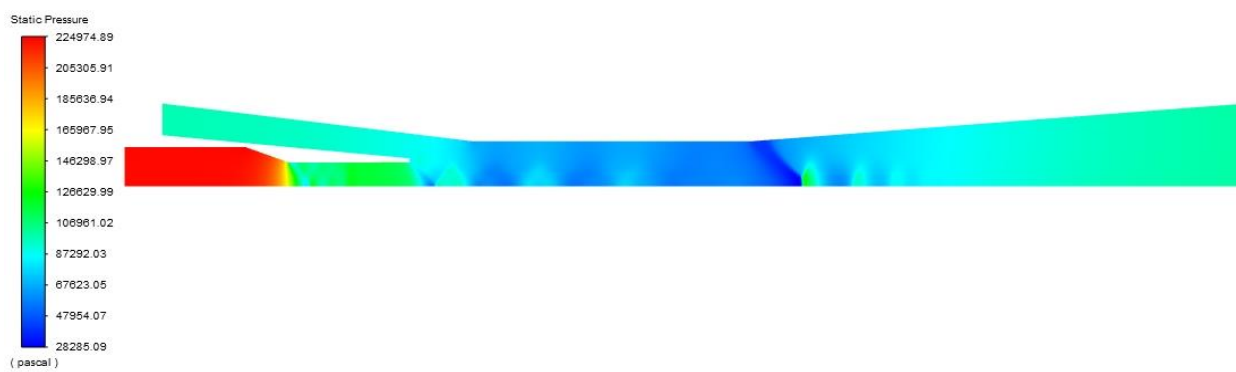


Fig. 7 Ejector static pressure contour

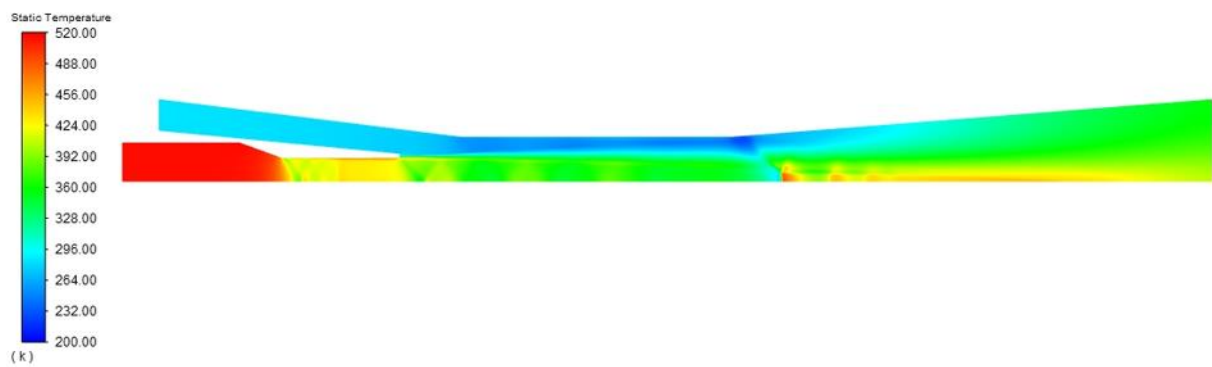


Fig. 8 Ejector static temperature contour

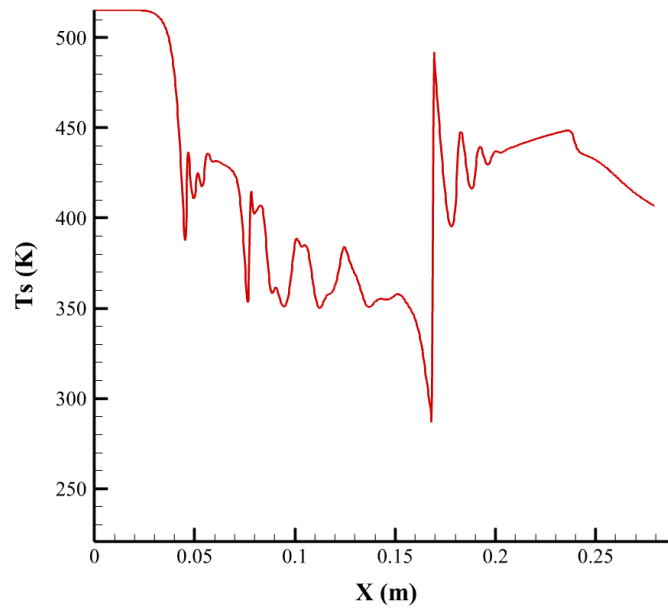


Fig. 9 Static temperature distribution along the ejector

Fig. 10 plots the pressure outlet changes concerning the suction ratio. According to it, increasing the pressure outlet value from 0.04 to 0.105 MPa did not cause changes in the suction ratio. The critical pressure for the model is equal to 0.105 MPa because raising the pressure outlet to more than that value has caused a sharp decrease in the suction ratio.

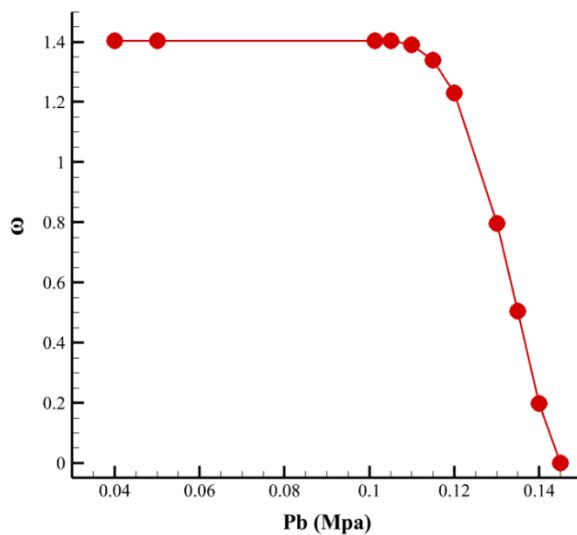


Fig. 10 Pressure outlet changes with the suction ratio in the ejector

Increasing the pressure outlet from the mentioned value has caused a sharp drop in

the suction ratio. Finally, for the last pressure (0.145 MPa), the suction ratio has reached zero. This means that the secondary fluid flow has reached zero or even flow in this channel has reversed, and the ejector is malfunctioning.

5- Conclusion

In this article, a supersonic ejector with a high-temperature primary fluid has been investigated. The purpose of this research is to investigate the secondary fluid suction, which enters the ejector from the free atmosphere. The primary and secondary fluid pressures were 520 and 2.3 bar, 288 and 1.01325 bar, respectively. Increasing the entrainment ratio means a higher suction of cooler fluid into the mixing chamber, which results in a lower ejector outlet temperature. The results revealed that in the throat of the primary nozzle, the flow reached supersonic and after that, a strong shock wave was created. Then, the flow passing through this part is involved in successive oblique and expansion shock waves, which finally reach the maximum Mach number at the end of the chamber. After the formation of a normal shock in

this portion, the flow at the diffuser inlet has reached subsonic. Also, the core of the jet flow from the primary nozzle outlet to the rear of the mixing chamber has become smaller. This is due to the suction of the secondary fluid and the interaction of this flow with the core of the main jet. In fact, the high energy and momentum of the core of the main jet are reduced by the secondary fluid suction. The temperature data also demonstrated that there are severe temperature changes inside the primary nozzle, which is the reason for the successive shocks. It was observed that the suction of the secondary flow in the mixing chamber causes the core of the main jet to become smaller in the center of the ejector. The increase in temperature after the normal shock has increased the outlet temperature from the center of the ejector.

References

- [1] Hart, John H.(2002). Supersonic ejector simulation and optimization. *PhD diss., University of Sheffield*.
- [2] Besagni, Giorgio, Riccardo Mereu, and Fabio Inzoli. (2016). Ejector refrigeration: A comprehensive review. *Renewable and Sustainable Energy Reviews*, 53, 373-407.
- [3] Omidvar, Amir, Mohsen Ghazikhani, and Seyed Mohammad Reza Modarres Razavi. (2015). CFD study of a variable geometry ejector using R600a to detect optimal geometry for ejector refrigeration system. *Modares Mechanical Engineering*, 15(5), 227-237.
- [4] Xing, Meibo, Jianlin Yu, and Xiaoqin Liu. (2014). Thermodynamic analysis on a two-stage transcritical CO₂ heat pump cycle with double ejectors. *Energy Conversion and Management*, 88, 677-683.
- [5] Li, Xinguo, Qilin Zhang, and Xiajie Li. (2013) A Kalina cycle with ejector. *Energy*, 54, 212-219.
- [6] Chong, Daotong, Junjie Yan, Gesheng Wu, and Jiping Liu. (2009). Structural optimization and experimental investigation of supersonic ejectors for boosting low-pressure natural gas. *Applied Thermal Engineering*, 29(14).
- [7] Chen, Haoying, Changpeng Cai, Shangbin Jiang, and Haibo Zhang. (2021). Numerical modeling on installed performance of turbofan engine with inlet ejector. *Aerospace Science and Technology*, 112.
- [8] Shi, Lei, Guojun Zhao, Yiyan Yang, Da Gao, Fei Qin, Xianggeng Wei, and Guoqiang He. (2019). Research progress on ejector mode of rocket-based combined-cycle engines. *Progress in Aerospace Sciences*, 107, 30-62.
- [9] Zhang, Caizhi, Leyuan Chen, Lei Lu, Yu Li, Dong Hao, Cheng Siong Chin, and Yinjun Qiao. (2023). The experiment and the control of hydrogen circulation of fuel cell based on of fuel ejector: A review. *International Journal of Hydrogen Energy*, 50, 1415-1431.
- [10] He, Yihe, Xiaojuan Shi, and Honghu Ji. "Optimal Design of Ejector Nozzle Profile with Internal and External Integrated Flow. (2024). *Aerospace*, 11(3), 184.
- [11] Kumar, Arvind, Surendra Kumar Yadav, Virendra Kumar, and Abhishek Kulkarni. (2024). A comprehensive exploration of ejector design, operational factors, performance metrics, and practical applications. *Journal of the Brazilian Society of Mechanical Sciences and Engineering*, 46(1), 39.
- [12] Samsam-Khayani, Hadi, Sang Youl Yoon, Mirae Kim, and Kyung Chun Kim. (2023). Experimental and numerical study on low-temperature supersonic ejector." *International Journal of Thermofluids*, 20.
- [13] Wang, Xiaoyan, Yufeng Zhang, Ye Tian, Xiaoqiong Li, Sheng Yao, and Zhangxiang Wu. (2021). Experimental investigation of a double-slider adjustable ejector under off-design conditions. *Applied Thermal Engineering*, 196.
- [14] Atmaca, Mustafa, and Cüneyt Ezgi. (2022). Three-dimensional CFD modeling of a steam ejector. *Energy Sources, Part A: Recovery, Utilization, and Environmental Effects*, 44(1), 2236-2247.
- [15] de Oliveira Marum, Victor Jorge, Livia Bueno Reis, Felipe Silva Maffei, Shahin Ranjbarzadeh, Ivan Korkischko, Rafael dos Santos Gioria, and Julio Romano Meneghini.

- (2021). Performance analysis of a water ejector using Computational Fluid Dynamics (CFD) simulations and mathematical modeling. *Energy*, 220 .
- [16] Chen, Haoying, Haibo Zhang, Zhihua Xi, and Qiangang Zheng. (2019). Modeling of the turbofan with an ejector nozzle based on infrared prediction, *Applied Thermal Engineering*, 159.
- [17] Ma, Xiaoli, Wei Zhang, S. A. Omer, and S. B. Riffat. (2010). Experimental investigation of a novel steam ejector refrigerator suitable for solar energy applications. *Applied Thermal Engineering* 30(11), 1320-1325.
- [18] Ruangtrakoon, Natthawut, Satha Aphornratana, and Thanarath Sriveerakul. (2011). Experimental studies of a steam jet refrigeration cycle: effect of the primary nozzle geometries to system performance. *Experimental thermal and fluid science*, 35(4), 676-683.
- [19] Sun, Da-Wen. (1997). Experimental investigation of the performance characteristics of a steam jet refrigeration system." *Energy Sources*, 19(4), 349-367.
- [20] Zhu, Yinhai, and Yanzhong Li. (2009). Novel ejector model for performance evaluation on both dry and wet vapors ejectors. *International journal of refrigeration* 32 (1), 21-31.
- [21] Yen, Ruey Hor, Bin-Juine Huang, Chien-Yu Chen, T. Y. Shiu, C. W. Cheng, S. S. Chen, and K. Shestopalov. (2013). Performance optimization for a variable throat ejector in a solar refrigeration system. *international journal of refrigeration*, 36(5), 1512-1520.
- [22] Chen, WeiXiong, Ming Liu, DaoTong Chong, JunJie Yan, Adrienne Blair Little, and Yann Bartosiewicz. (2013). A 1D model to predict ejector performance at critical and sub-critical operational regimes. *International journal of refrigeration*, 36(6), 1750-1761.
- [23] A. Omidvar, M. Ghazikhani, M. R. M. Razavi, (2014). CFD study of a variable geometry ejector using R600a to detect optimal geometry for ejector refrigeration system, *Modares Mechanical Engineering*, 15(5), 227-237.
- [24] Lew, Adrián J., Gustavo C. Buscaglia, and Pablo M. Carrica. (2001). A note on the numerical treatment of the k-epsilon turbulence model. *International Journal of Computational Fluid Dynamics*, 14(3), 201-209.
- [25] Richards, P. J., and R. P. Hoxey. (1993). Appropriate boundary conditions for computational wind engineering models using the k- ϵ turbulence model. *Journal of wind engineering and industrial aerodynamics*, 46, 145-153.
- [26] Shahriari, Behrooz, and Mohammad Reza Hashemi. (2023). Numerical solution of hovering propeller performance at various blade pitch angles and revolutions with different turbulence models. *Journal of Simulation and Analysis of Novel Technologies in Mechanical Engineering*, 15(4), 5-15.
- [27] Chong, Daotong, Mengqi Hu, Weixiong Chen, Jinshi Wang, Jiping Liu, and Junjie Yan. (2014). Experimental and numerical analysis of supersonic air ejector. *Applied Energy*, 130, 679-684.